Influence of Shim Layers on Progressive Failure of a Composite Component in Composite-Aluminum Bolted Joint in Aerospace Structural Assembly

Cephas Yaw Attahu[1], *An Luling*[1*], *Li Zhaoqing*[2], *Gao Guoqiang*[1]

1. Department of Aerospace Manufacturing Engineering, Jiangsu Key Laboratory of Precision and Micro-Manufacturing Technology, Nanjing University of Aeronautics and Astronautics, Nanjing 210016, P. R. China;
2. AVIC Xi'an Aircraft Industry (Group) Company LTD, Xi'an 710089, P. R. China

(Received 26 December 2016; revised 19 June 2017; accepted 23 June 2017)

Abstract: The influence of varying shim layers on the progressive damage/failure of a composite component in a bolted composite-aluminum aerospace structural assembly was investigated using a non-linear three-dimensional (3D) structural solid elements assembled model of a carbon fiber-reinforced polymer (CFRP)-aluminum single-lap joint with a titanium (Ti-6Al-4V) fastener and a washer generated with the commercial finite element (FE) software package, ABAQUS /Standard. A progressive failure algorithm written in Fortran code with a set of appropriate degradation rules was incorporated as a user subroutine in ABAQUS to simulate the non-linear damage behavior of the composite component in the composite-aluminum bolted aerospace structure. The assembled 3D FE model simulated, as well as the specimen for the experimental testing consisted of a carbon-epoxy IMS-977-2 substrate, aluminum alloy 7075-T651 substrate, liquid shim (Hysol EA 9394), solid peelable fiberglass shim, a titanium fastener, and a washer. In distinction to previous investigations, the influence of shim layers (liquid shim and solid peelable fiberglass shim) inserted in-between the faying surfaces (CFRP and aluminum alloy substrates) were investigated by both numerical simulations and experimental work. The simulated model and test specimens conformed to the standard test configurations for both civil and military standards. The numerical simulations correlated well with the experimental results and it has been found that: (1) The shimming procedure as agreed upon by the aerospace industry for the resolution of assembly gaps in bolted joints for composite materials is the same for a composite-aluminum structure; liquid shim series (0.3, 0.5 and 0.7 mm thicknesses) prolonged the service life of the composite component whereas a solid peelable fiberglass shim most definitely had a better influence on the 0.9 assembly gap compared with the liquid shim; (2) The shim layers considerably influenced the structural strength of the composite component by delaying its ultimate failure thereby increasing its service life; and (3) Increasing the shim layer's thickness led to a significant corresponding effect on the stiffness but with minimal effect on the ultimate load.

Key words: composite-aluminum; progressive failure modeling; finite element modeling; single-lap bolted joint; shimming; aerospace structures

CLC number: V241 **Document code**: B **Article ID**: 1005-1120(2018)01-0188-15

0 Introduction

Due to their high specific stiffness, higher specific strength and other better performances, composite materials are hugely being utilized in the aerospace industries for both civil and military applications[1,2]. Although composite materials are extensively being used because of the aforementioned reasons, composite structures are susceptible to damage as a result of their brittle nature and other technical issues like shimming[3,4]. Aluminum alloys, however, are still being used in the aerospace industry despite the growing usage of composite materials. An example of the

* Corresponding author, E-mail address: anllme@nuaa.edu.cn.

How to cite this article: Cephas Yaw Attahu, An Luling, Li Zhaoqing, et al. Influence of shim layers on progressive failure of a composite component in composite-aluminum bolted joint in aerospace structural assembly[J]. Trans. Nanjing Univ. Aero. Astro., 2018,35(1):188-202.
http://dx.doi.org/10.16356/j.1005-1120.2018.01.0188

use of hybrid materials (that is composite-metal structures) is the fighter jet JAS39 Gripenas shown in Fig. 1[5]. Furthermore, some aircraft manufacturers like Airbus still maintain a significant percentage of aluminum alloys in its manufactured aircrafts (A320′s airframe is composed of aluminum alloy) which make the assembly of hybrid structures (composite-aluminum) inevitable. In the assembly of aerospace structural components, there are several mechanical fasteners employed and as a result, holes have to be drilled for the installation of these mechanical fasteners. Before starting to drill the hole and with subsequent fastener installation, it is imperative to check all joints for the presence of gaps. This is because the presence of gaps can needlessly preload the metallic members when fasteners are installed prompting a condition that can cause premature fatigue cracking and even stress corrosion cracking of an aluminum component. Howbeit, gaps in structures containing composites can cause even more serious problems than in metallic structures. Since composites do not yield and are more brittle and less lenient than metals, excessive gaps can result in delaminations when they are pulled out during fastener installation.

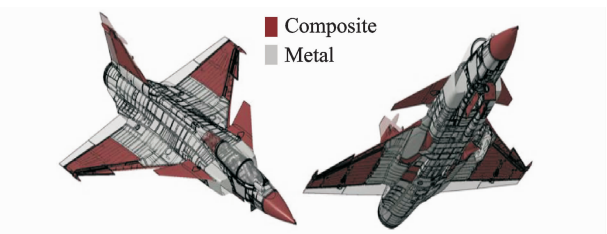

Fig. 1 Composite and metal materials in JAS39 Gripen

This phenomenon put the composite in a bending due to the exerted force by the fastener drawing the parts together and can develop matrix cracks and/or delaminations around the holes. Cracks and delaminations normally occur in multiple layers through the thickness and can significantly affect the joint strength[6].

There have been several studies into the progressive failure of composite materials. Tsai and Wu[7]; Reddy and Pandey[8]; Turvey[9]; and Hashin[10] revolutionized the studies into the progressive failures of composite materials. Other authors like Chang and Chang[11] developed the progressive damage analysis of notched laminated composites subjected to tensile loading. The progressive failure method employed in Ref. [11] was a nonlinear FEA that used the modified Newton-Raphson iteration technique to develop the state of stresses in a composite component. Also, Chang and Lessard[12] conducted an investigation into the damage in laminated composites containing an open hole subjected to a compressive loading. Contributing to the advances in failure theories of composite materials, Reddy et al.[13] evaluated both linear and non-linear first-ply failure loads of composite plates for different edge conditions and load cases. The apparent complexities associated with composite materials made the aforementioned failure theories to have had limitations which necessitated and motivated other authors to further refine these existing theories. An example of a refined theory for the progressive failure analysis of composite materials has been developed and successfully implemented in the works of Ref. [14].

There has been some published literature on shimming[15-17], but most studies were skewed toward liquid shims[18-22]. With regard to the analysis of failure of composite materials with ashim, the authors Hühne et al.[18]; Dhôte et al.[19]; Comer et al.[20]; and Liu[22] conducted studies using single-lap bolted joints with a liquid shim. In investigations of Ref. [22], in particular, it was concluded that the stiffness of the joints decreased due to the presence of liquid shim, and the joint stiffness decreased with an increasing liquid shim thickness. Comer et al.[20] investigated thermo-mechanical fatigue tests on hybrid joints with liquid shim layers and concluded that there was no degradation in respect to the mechanical stiffness for the liquid shim. Zhai et al.[23] studied the effect of solid shim and liquid shim on composite-aluminum bolted joints by using a 3D Digital Image Correlation. Although, the investigation of Ref. [23] was "supposed" to be about solid shim and liquid shim, however, it

was carried out experimentally hence the objective of this research to investigate the influence of both liquid and solid peelable fiberglass shim using finite element analysis and experimental study.

1 Materials for Experimental Testing and Finite Element Modeling of Composite-Aluminum Bolted Joint

The 3D finite element (FE) assembled model and the test specimens were an idealization of an aircraft′s wingbox sub-structural components. That is a composite wing panel and an aluminum rib. Aluminum alloy 7075-T651 was chosen for this study because of its use in the aerospace industry for highly stressed and critical structural parts[6,7]. The test specimens, as well as the FE model, were composed of the parts (Figs. 2,3): A hi-shear corporation fastener with a protruding head (HST-12-8) and a washer all composed of aerospace grade titanium alloy (Ti-6Al-4V-STA); one plate made of the carbon fiber-reinforced polymer (CFRP) material-carbon-epoxy IMS-977-2 (Cytec Industries Inc.) with the quasi-isotropic stacking sequence being $[+45/90/-45/0/90/0/-45/90/+45/-45]_s$ and with a total ply thickness of 0.188 mm for 20 plies; the other plate is made of a high strength aerospace grade aluminum alloy, 7075 T651. Two CFRP support plates were adhesively bonded to the main plates to avoid excessive bending. Commercially available liquid shim material-Hysol EA9394 of Henkel Corporation and a solid peelable fiberglass of LAMECO group manufactured under the COMAC standard CMS-MT-301 were the other materials utilized. The FE model and the test specimens were based on the test standards of American Society for Testing and Materials (ASTM), D5961/D5961M-13[24] and recommendations in Ref. [20]. The single-lap model of the composite-aluminum bolted joint specimen is shown in Figs. 2,3.

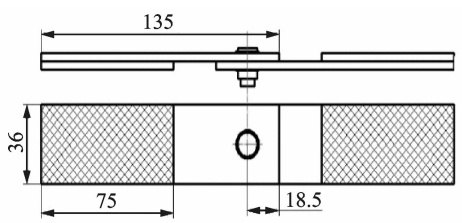

Fig. 2 Dimensions in millimeter of the single-lap

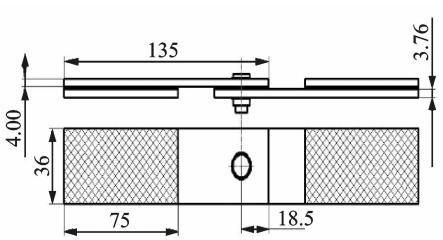

Fig. 3 Dimensions in millimeter of the single-lap composite-composite-aluminum bolted joint without shim aluminum bolted joint with shim

2 Finite Element Model

A non-linear 3D solid elements model of a single-lap composite-aluminum assembled structure with and without shim layers under a quasi-static tensile loading was developed using the commercial FE program ABAQUS/Standard 6.13[25] and in accordance with Refs. [20,24]. The developed model was without the doublers as shown in Fig. 4. The bolt, collar, and the washer were modeled as a unit as shown in Fig. 5 because they were engaged together and they are composed of the same titanium material. There were nine different kinds of composite-aluminum bolted joints. Namely, without a shim, with a liquid shim (0.3, 0.5, 0.7 and 0.9 mm thickness) and with solid peelable fiberglass (0.3, 0.5, 0.7 and 0.9 mm thickness).

The strength and elastic properties[26] for the carbon-epoxy IMS-977-2 substrate are shown in Table 1. The meshed CFRP had a total number of 37 040 elements after it has been seeded with 20 elements in the thickness direction, 15 elements equally distributed in the area covered by the fastener head and 20 elements equally distributed on the half periphery of each fastener hole along the circumferential direction. Structured hexagonal mesh controls were assigned and a stack direction assigned in the isometric view. The meshed CFRP plate as shown in Fig. 6 was developed using the element type C3D8R: An eight-node linear brick, reduced integration, hourglass control in Abaqus.

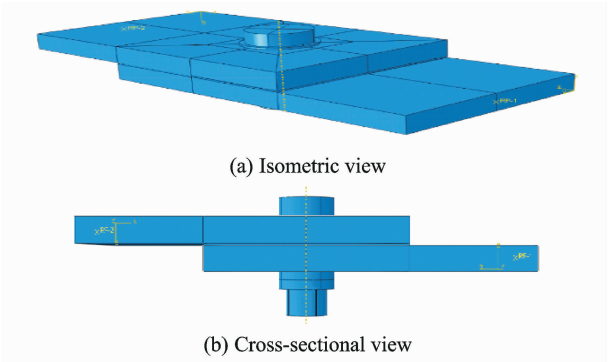

Fig. 4 Developed model

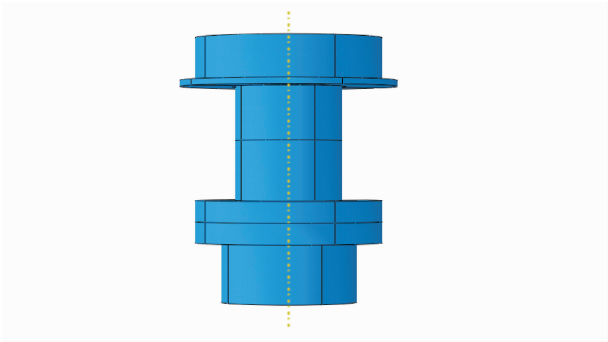

Fig. 5 FE model of bolt-collar-washer

Table 1 CFRP elastic and strength properties

Property		Value
Longitudinal modulus	E_{11}/GPa	156
Transverse modulus	E_{22}/GPa	8.35
Out-of-plane modulus	E_{33}/GPa	8.35
In-plane shear modulus	G_{12}/GPa	4.2
Out-of-plane shear modulus	G_{13}/GPa	4.2
Out-of-plane shear modulus	G_{23}/GPa	2.52
In-plane Poisson′s ratio	v_{12}	0.33
Out-of-plane Poisson′s ratio	v_{13}	0.33
Out-of-plane Poisson′s ratio	v_{23}	0.55
Longitudinal tensile strength	X_T/MPa	2 500
Longitudinal compressive strength	X_C	1 400
Transverse tensile strength	Y_T	75
Transversecompressive strength	Y_C	250
Out-of-plane tensile strength	Z_T	75
Out-of-plane compressive strength	Z_C	250
In-plane shear strength	s_{12}	95
Out-of-plane shear strength	s_{13}	95
Out-of-plane shear strength	s_{23}	108

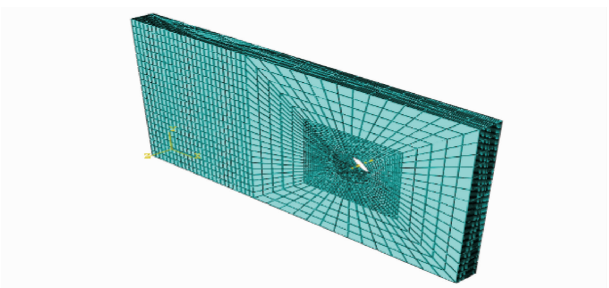

Fig. 6 CFRP meshed FE model

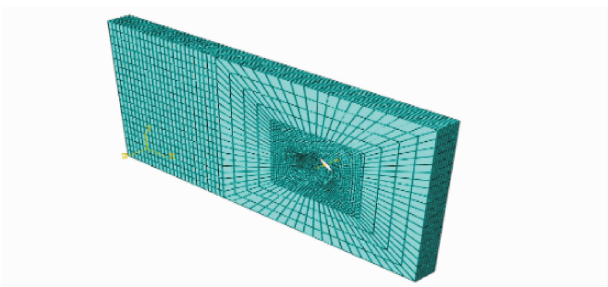

Fig. 7 AA7075-T651 meshed FE model

The aluminum plate and titanium parts were modeled using their elasto-plastic material behaviors as shown in Table 2. The AA7075-T651 was modeled same as the CFRP with the only differences being the seeding in the thickness direction where 10 elements were used and there was no assigning of stacking direction. The meshed AA7075-T651 plate in Fig. 7 has a total number of 17 520 elements. Titanium parts (meshed Ti-6Al-4V STA is shown in Fig. 8) were modeled same as the CFRP but with different approximate global size (0.6 used) and mesh controls (sweep used).

The Hysol EA9394 of Henkel Corporation and the solid peelable fiberglass were modeled using their elastic properties as shown in Table 3. The shim materials (an example shown in Fig. 9 is a meshed model of a shim with a thickness

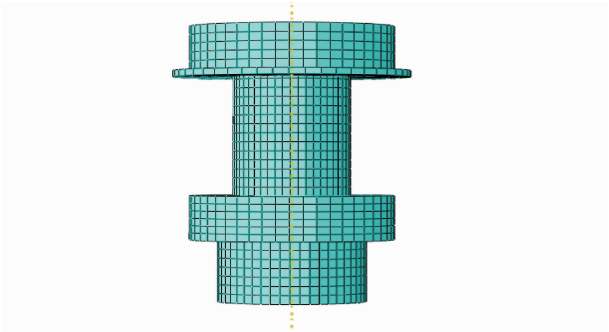

Fig. 8 Bolt-collar-washer meshed FE model

of 0.3 mm) were also modeled same as the CFRP but with an approximate global size of 0.7and seeded with 3 elements in the thickness direction for a shim thickness of 0.3 mm (5 elements and 7 elements for shim thickness of 0.5 mm and 0.7 mm, respectively).

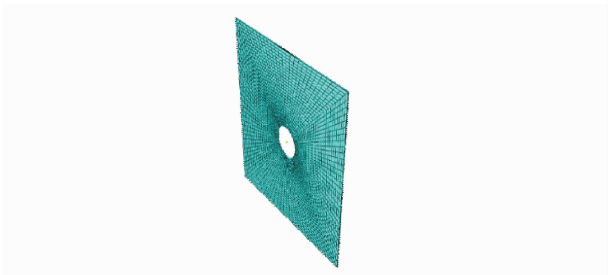

Fig. 9 Shim material meshed FE model

Table 2 Elasto-plastic properties of AA7075-T651[27] and Ti-6Al-4V STA[14]

Material	Young's modulus E/MPa	Poisson's ratio v	Yield stress σ_y/MPa	Plastic strain ε_p
AA7075-T651	71 700	0.306	490	0
			501	0.002
			561	0.09
Ti-6Al-4V STA	110 000	0.29	950	0
			1 034	0.002
			1 103	0.1

Table 3 Elastic properties of Hysol EA9394[28] and solid peelable fiberglass[29]

Property	Hysol EA9394	Solid peelable fiberglass
Young's modulus/MPa	4 330	84 700
Poisson's ratio v	0.35	0.24

The boundary conditions of the FE model in Fig. 10 has the "Reference Node 2" (RP-2) which is the aluminum plate held fixed in all six degrees of freedom (U_x, U_y, U_z, R_x, R_y and R_z) because it is clamped and the "Reference Node 1" (RP-1) which is the CFRP plate held fixed in two translational directions (U_y and U_z) and in all three rotational directions (R_x, R_y and R_z). A pull distance of 10 mm was then applied to RP-1 in the U_x direction.

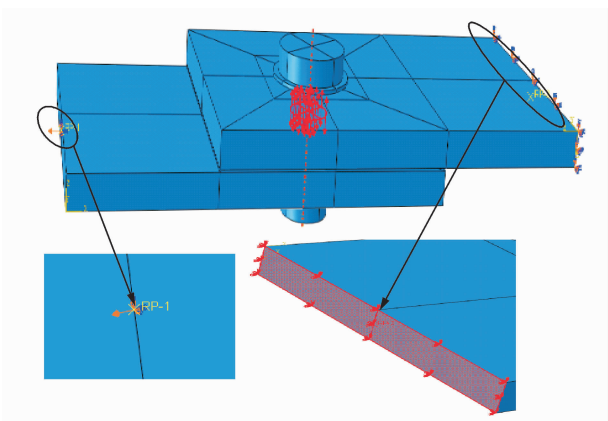

Fig. 10 Boundary conditions on the plates

The clamping force of 10 kN[30] produced by the tightening torque was applied through a bolt load function as shown in Fig. 11 in ABAQUS. The contact relationships were defined for contact pairs interacting with each other using a stringent master-to-slave rule[25]. A total of six contact pairs were defined and implemented in the FE model under the interaction section in Abaqus. Contact was modeled between (a) the main plates, (b) between fastener (shanks) and plate holes, (c) between shim, plates, fastener shanks and plate holes, (d) between aluminum plate and

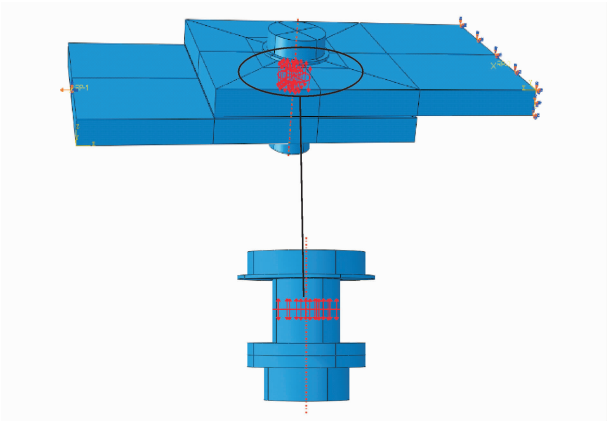

Fig. 11 Bolt load application

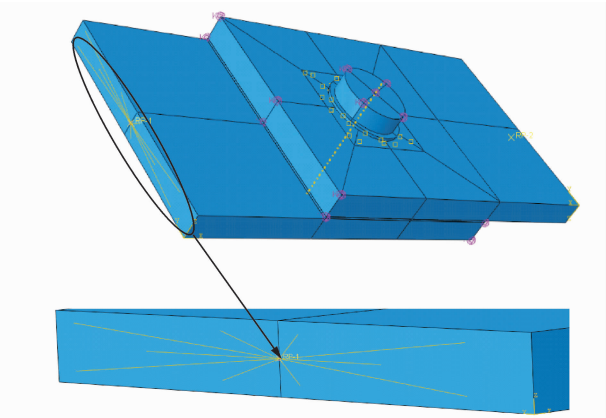

(a) Upper surfaces of the assembled model

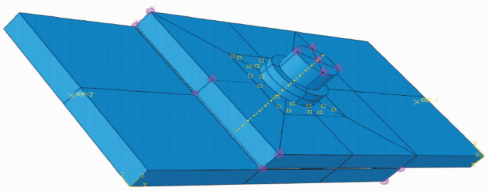

(b) Bottom surfaces of the assembled model

Fig. 12 Boundary conditions on the assembled model

washer (bottom surface) and (e) between collar (upper surface) and composite plate. The contacts were defined using the penalty method with hard contact, friction, and finite sliding. "Finite-Sliding" allows for any arbitrary motions of the faying surfaces and the active contact constraints any changes during the analysis. "Small-Sliding" is used if there is a relatively little sliding of any surfaces interacting with each other. A surface-to-surface contact option was used for all contacts, several coefficients of friction were used in the model and their value depended on the components in contact. The frictional coefficient for the interaction between the composite plate and the titanium parts: 0.16[30]. Frictional coefficients of 0.288[31] and 0.235[32] were used for interactions between aluminum plate and titanium parts, and between composite plate and aluminum plate, respectively. The additional frictional coefficient which is 0.2 (assumed), was assigned to all other parts interacting with the shim materials. The surface of the modeled shim was tied onto the composite plate and as shown in Fig. 12, special elements (springs/dashpots) were used to connect points to ground. RP-1 was used to create a set (set-coupling) and with set-coupling as the control points, a constraint (coupling kinematic-type) was created using the surface on which RP-1 was situated.

With this done, the set-coupling was used to generate the needed FEA results for analysis.

3 Progressive Damage Modeling of CFRP

Damage in composite structures is internally initiated and accumulated over a period of time before structural failure. The use of failure criteria alone to predict the ultimate failure is not enough because the failure criteria predict the onset of the damage occurring hence there is the need to develop an algorithm to simulate the nonlinear material behavior in the composite structure. The developed algorithm: The progressive damage, is based on the ply-discount method. The failure modes with their criterion; and the material property degradation rules used in the progressive damage model (PDM) are adequately documented in Ref. [14]. The PDM is an integration of the stress analysis, failure analysis, and material property degradation. The flowchart for the progressive failure algorithm[33] is shown in Fig. 13 and the following steps give a detailed explanation of the flowchart:

Step 1 The development of the 3D solid FE model of the composite-aluminum bolted structure by inputting the various material properties,

boundary conditions, contacts, initial load and final load step.

Step 2 Non-linear stress analysis is performed.

Step 3 Failure analysis is performed by applying the failure criteria.

Step 4 Ply failures are checked:

(1) If no failure is predicted, the applied load, F^m is increased by an increment, ΔF according to the equation: $F^m = F^{m-1} + \Delta F$, and the program goes back to Step 2.

(2) If there is a mode of failure being predicted, then the program moves on to the next step.

Step 5 The degradation of the material properties of the plies that had failed.

Step 6 Final failure checking:

(1) If the final failure is reached, the program stops.

(2) If not, the program goes back to Step 2 and the non-linear stress analysis is carried out again so as to calculate the redistributed stresses. Convergence at a load step is assumed (is proved to be a good compromise between accuracy and time consumption)[34] when no additional failure is detected.

The PDM written in FORTRAN was implemented into Abaqus/Standard as a user-defined subroutine, USDFLD. The degradation rules were implemented using the field variables (FV) which are dependent on the failure criterion of each failure mode. The USDFLD, within ABAQUS, provides the user a method to write a program that updates the FV at every integration point for each increment in the analysis according to the failure criteria values obtained during the solution.

At the beginning of each increment, the USDFLD, using the utility subroutine GETVRM, accesses the material point quantities for every integration point in the model and these solution-dependent field variables (SDV) are then used to create an array of FVs to define the material properties of the next iteration[34]. Additional, solution-dependent state variables (STATEV), which provide a dependence of each material point on its history, may be updated in this subroutine and the updated values are then passed to another user subroutines that are called at the material point. These state variables are eventually transferred back into the main Abaqus program. According to the different failure modes, there are four different state variables which are defined to display the progression of damage during the post-processing. The failure modes simulated are matrix failure (FV1), fiber failure (FV2), fiber-matrix shear failure (FV3) and shear non-linearity (FV4). After the stress analysis, the generated stress values are then used to compute the failure criterion values. If any of the values are greater or equal to 1, the related field variable for the integration point with the highest failure criterion value is set permanently to 1, which indicates failure (it is important to note that the degradation models implemented within ABAQUS degrade at the integration points rather than elements). And these solution-dependent field variables are then used to define the material properties of the next iteration.

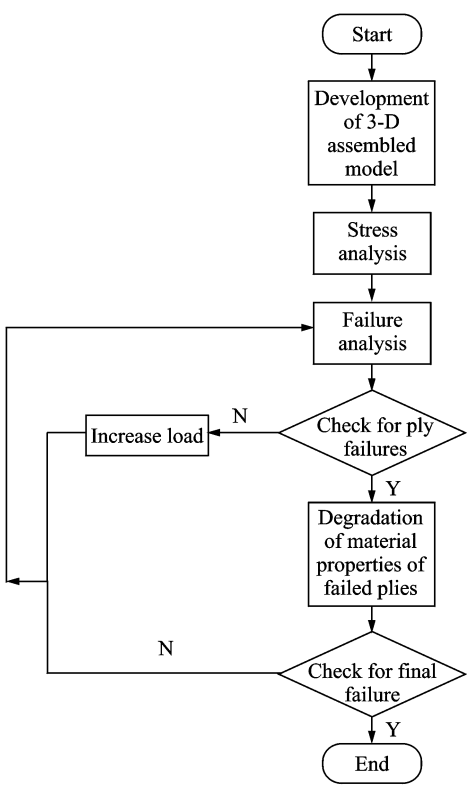

Fig. 13 Flowchart of the progressive damage algorithm

4 Experimental Work

The test specimens consisted of two plates (composite and aluminum), shim materials (liquid shim-Hysol EA9394 and solid shim-peelable fiberglass) and a prestressed titanium bolt with a protruding head. The experiment was performed under quasi-static tensile loading using an electronic universal testing machine (SANS 4105). The test machine was manufactured in accordance with the GB/T 228-2002 code of Chinese National Standards. The tests were conducted at a loading velocity of 10 mm/s at room temperature.

4.1 Test specimen preparation

The specimen in Fig. 14 was prepared in accordance with the configurations in Refs. [20, 24]. The liquid shim was prepared in accordance with the manufacturer's instructions and applied to the composite plate. The prepared specimens were clamped and allowed at least four days to cure at room temperature. Finally, the plates were fastened together by the torquing off of the collars with finger-tightening.

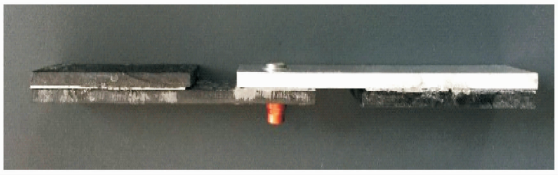

Fig. 14 Composite-aluminum bolted structure

For the specimen with shim materials, the shim adhered to the mating surface of the composite plate, as shown in Figs. 15,16, for a specimen with a liquid shim and a solid shim, respectively. The specimen without any shim is also shown in Fig. 17.

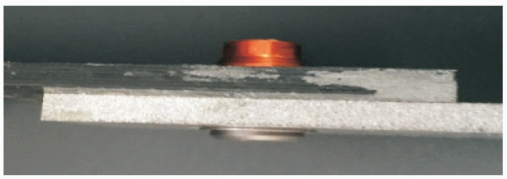

Fig. 15 Test specimen with a liquid shim

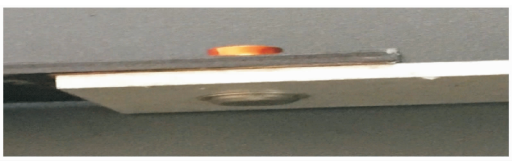

Fig. 16 Test specimen with a solid shim

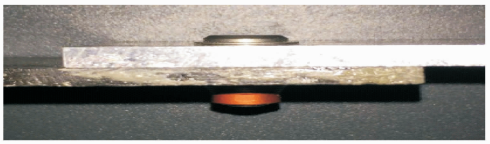

Fig. 17 Test specimen without shim

4.2 Test set-up and procedure

The test specimens were rigidly clamped into the testing machine as shown in Fig. 18. The load application was carried out with a constant traverse speed until structural collapse occurred.

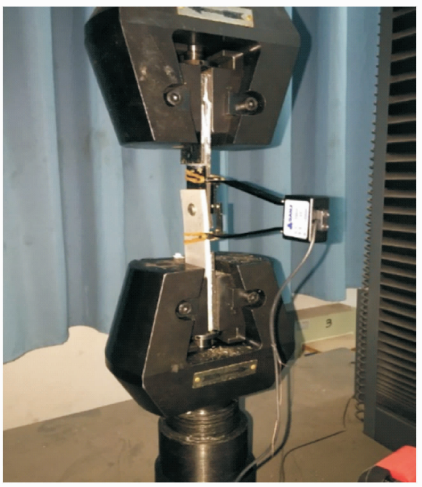

Fig. 18 Test specimen rigidly clamped into the testing machine

The force against the displacement of the specimens was recorded by a computer. Fig. 19

Fig. 19 Test set-up for the experiment

shows the experimental arrangement.

The experiments were stopped after the load had dropped to 15% of its peak load or after the occurrence of an excessive displacement. Each test configuration was repeated with three test specimens and the results that corresponded accurately with the FE results has been presented in this paper.

5 Results and Discussion

The numerically simulated results were compared with the experimental data and they were in agreement very well with each other. Subsequently discussed are the load-displacement behavior and the influence of the shim layers on the damage behavior of the composite component. The test results are shown in Figs. 20 (a—e) and Figs. 21 (a—e).

5.1 Load-displacement evaluation

The numerically simulated load-displacement behavior of the composite component was very similar with the experimentally determined data. Figs. 20 (a—e) show the load-displacement curves for specimen without shims, 0.3, 0.5, 0.7 and 0.9 mm shim thickness, respectively (both liquid and solid shim).

The maximum experimentally determined load for a specimen without any shims was 16.09 kN at a displacement of 6.1 mm but the maximum experimentally determined load for a specimen with a 0.3 mm liquid shim thickness was 19.83 kN at a displacement of 9.7 mm. And also, the maximum experimentally determined load for a specimen with a 0.3 mm solid shim thickness was 18.60 kN at a displacement of 7.9 mm. This kind of trend where all the maximum experimentally determined loads and displacements for specimens with shims being higher than the maximum experimentally determined loads and displacements for specimen without any shims is also obviously seen in Fig. 20. The reason for such an observation is the presence of shim. The presence of shims increased the amount of load needed for failure and also increased the strength of the component by increasing the displacement at which failure occurs.

A further examination of the test results reveals that, with regard to the load-displacement evaluation, the simulated load values were higher than the experimentally determined load values at the same displacement and the differences in these values could be as a result of several factors but predominately, it could be the: (1) Differences in material properties used in the FE modeling and the "actual properties" of the test specimen; (2) Inherent limitations of the failure method used to simulate the damage; and (3) Degradation rules being somewhat different from the "actual failure progression" of the test specimen.

The progression of the load-displacement curves for the simulated conditions and the experimental conditions were as a result of friction so, the choice of the frictional coefficient to be used for modeling is very important. It has been observed that there is a linearity in the behavior of the composite component initially before reaching the peak loads and subsequently experiencing large displacements before failure. The progressive damage causes such a non-linear curve pattern until the ultimate load was reached. However, the ultimate load identified in the experiments could not be achieved exactly numerically. In comparison, the specimens with liquid shim series were a better fit for gap thickness of 0.3, 0.5, 0.7 mm whereas specimens with solid shim series were better situated for the gap thickness of 0.9 mm.

5.2 Influence of shim layer

To be able to estimate the influence of the shim layers on the damage of the composite component, it is imperative to plot the stiffness-load curves. Figs. 21 (a—e) show the stiffness-load curves for specimen without shims, with 0.3, 0.5, 0.7, 0.9 mm (both liquid and solid shim) shim thickness, respectively.

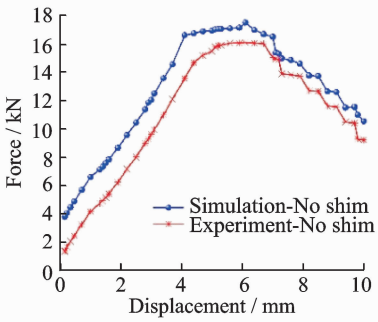

(a) Without shims

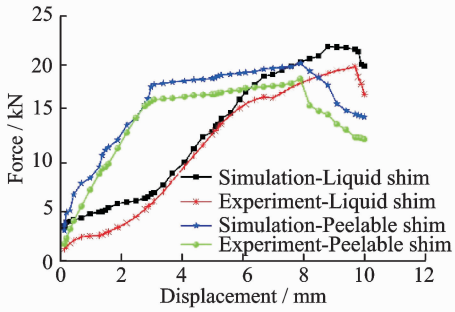

(b) With a 0.3 mm shim thickness

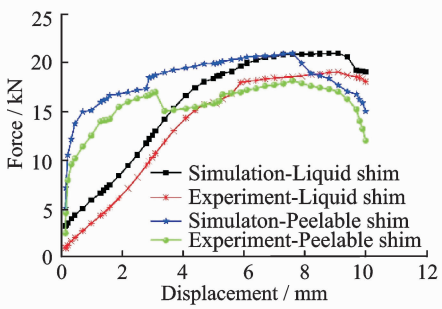

(c) With a 0.5 mm shim thickness

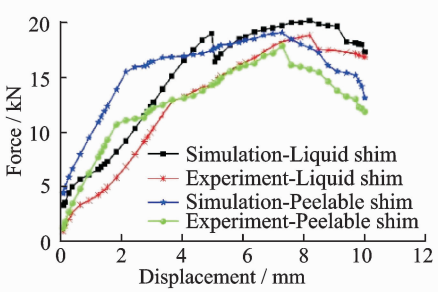

(d) With a 0.7 mm shim thickness

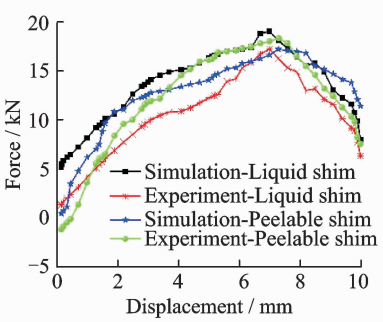

(e) With a 0.9 mm shim thickness

Fig. 20 Load-displacement trends for specimens without shim and with different shim thicknesses

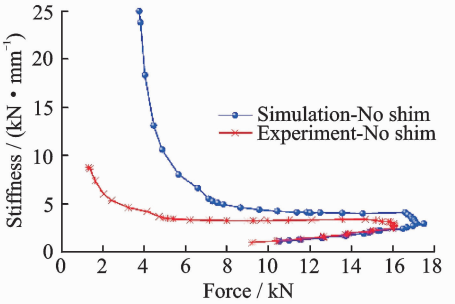

(a) Without shims

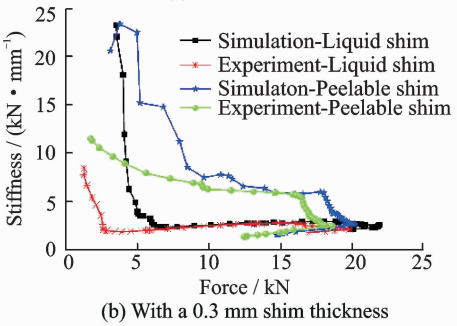

(b) With a 0.3 mm shim thickness

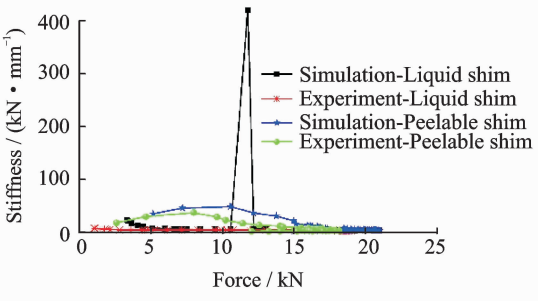

(c) With a 0.5 mm shim thickness

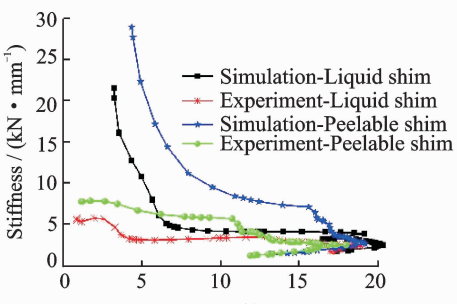

(d) With a 0.7 mm shim thickness

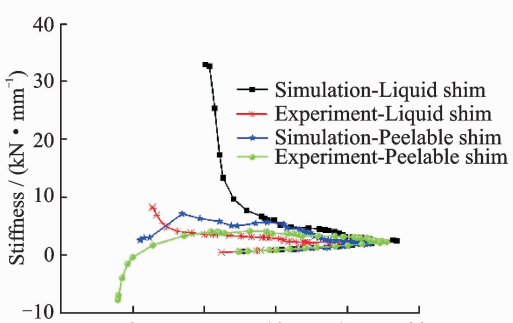

(e) With a 0.9 mm shim thickness

Fig. 21 Stiffness-load trends for specimens without shim and with different shim thicknesses

As shown in Figs. 21 (a—d), generally, the stiffness for both the experiment and that of the numerical simulation decreased with an increasing load up to the failure point of the component before gradually also decreasing with a decreasing load. As for Fig. 21(e), the stiffness for both the experiment and that of the numerical simulation decreased with an increasing load up to the failure point of the component before gradually also decreasing with a decreasing load for the liquid shim specimen but for the solid shim specimen, the stiffness gradually increased with an increasing load up to about a displacement of 2.0 mm before eventually decreasing with an increasing load up to the component's failure point and then finally decreased with a decreasing load. Probing further the curves in Fig. 20, it was obvious that with regard to the stiffness-load evaluation, the simulated stiffness values were higher than the experimentally determined stiffness values and it is much significantly higher for the about first six stiffness values. The differences in these values could be as a result of the factors discussed in Section 5.1.

The variations observed in Figs. 21 (a—e) are predominately due to the dissipation of friction which magnifies the fact that the choice of the coefficient of friction for the FE modeling is important. Afterward, the damage evolution starts and the linear stiffness decreases yield meant that some elements were completely damaged while others still had some stiffness in them. The specimen without any shim material generally exhibited higher stiffness than all liquid shim series (with the exception of 0.9 mm shim thickness) and all solid shim series (with the exception of 0.3 mm shim thickness and 0.5 mm shim thickness).

It is also clear from Figs. 21 (a—e) that, the use of liquid shim generally caused a reduction in the joint stiffness for 0.3, 0.5, 0.7 mm shim thickness. It is worth noticing that the solid shim was a better fit for the 0.9 mm shim thickness because it considerably gave a better stiffness degradation performance and this may be as a result of the higher tensile modulus of the solid peelable fiberglass shim. Fig. 22 shows the damaged specimens after the experiments.

Fig. 22 Damaged specimens

To demonstrate the "somewhat limitations" of the PDM used in simulating the damages, a closer look was taken at the damages for the test specimen without any shim material and the 0.3 mm shim thickness (both liquid and solid shim) as an illustration. The damages for the test specimen without any shim material and the 0.3 mm shim thickness (both liquid and solid shim) are shown in Figs. 23 (a—c), respectively.

(a) Without shims

(b) With a liquid shim

(c) With a solid shim

Fig. 23 Damaged specimens without shim and with liquid and solid shims

In the numerical simulation, the failure modes matrix failure, fiber failure as well as the fiber-matrix failure could be displayed but the shear non-linearity could not be "adequately" displayed because the FE-model is an idealization of the reality hence some assumptions were made. Those assumptions definitely had an effect on the actual damage. The view taken for the simulated damaged images is shown in Fig. 24.

Figs. 25(a—c), Figs. 26 (a—c), Figs. 27 (a—c) and Figs. 28(a—c) show the simulated

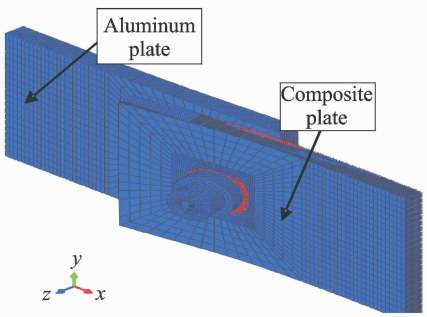

Fig. 24 View used for taking FV1, FV2, FV3 and FV4 damages

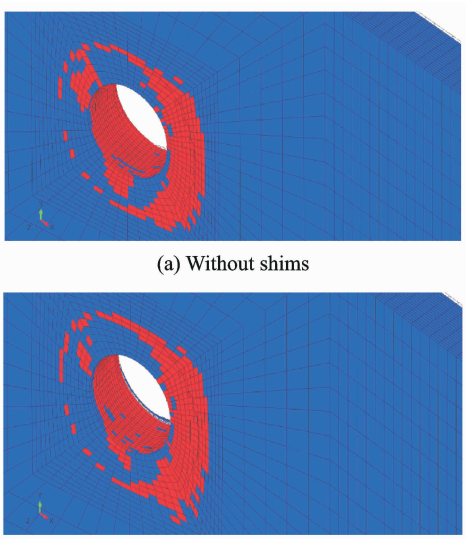

Fig. 25 FV1 damage for specimens without shim and with liquid and solid shim thicknesses

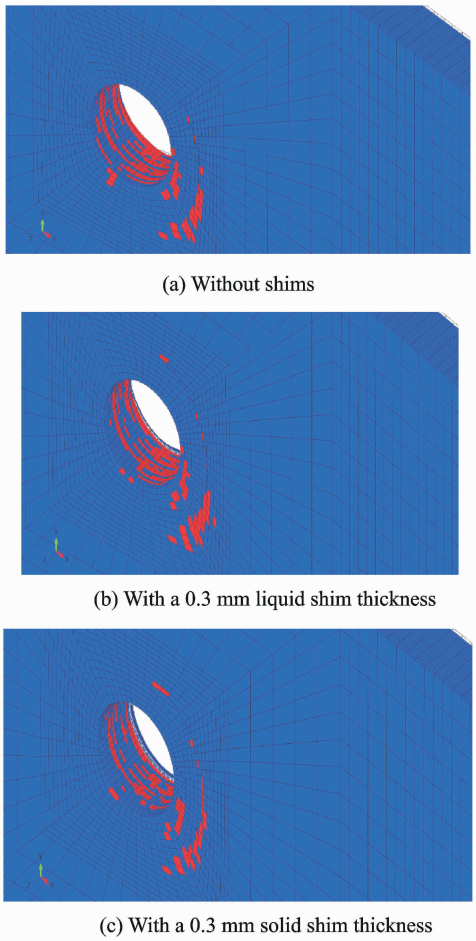

Fig. 26 FV2 damages for specimens without shim and with liquid and solid shim thicknesses

four damages (FV1, FV2, FV3, and FV4, respectively) for the specimen with no shim material, with a 0.3 mm liquid shim thickness, and with a 0.3 mm solid shim thickness.

In addition to an earlier explanation as to why the shear non-linearity damages in Figs. 28(a—c) could not be "adequately" displayed, it should be noted that it has been assumed in the theory being used in simulating the shear non-linearity that, the non-linearity mainly was caused by the micro-cracking in the matrix and the PDM could not simulate "such micro-cracking".

6 Conclusions

A three-dimensional finite element model of a single-lap, single-bolt composite-aluminum assembled structure has been developed to investi-

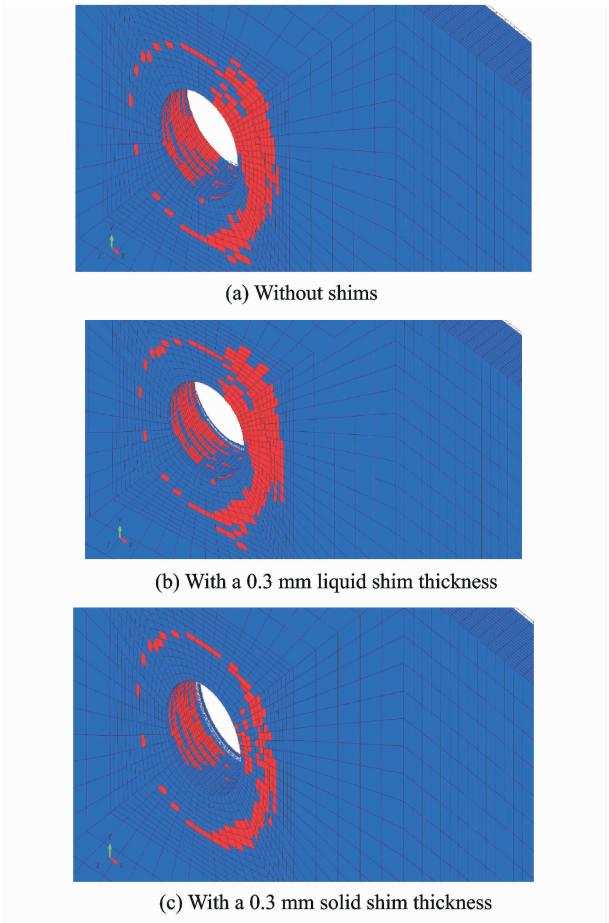

Fig. 27 FV3 damages for specimens without shim and with liquid and solid shim thicknesses

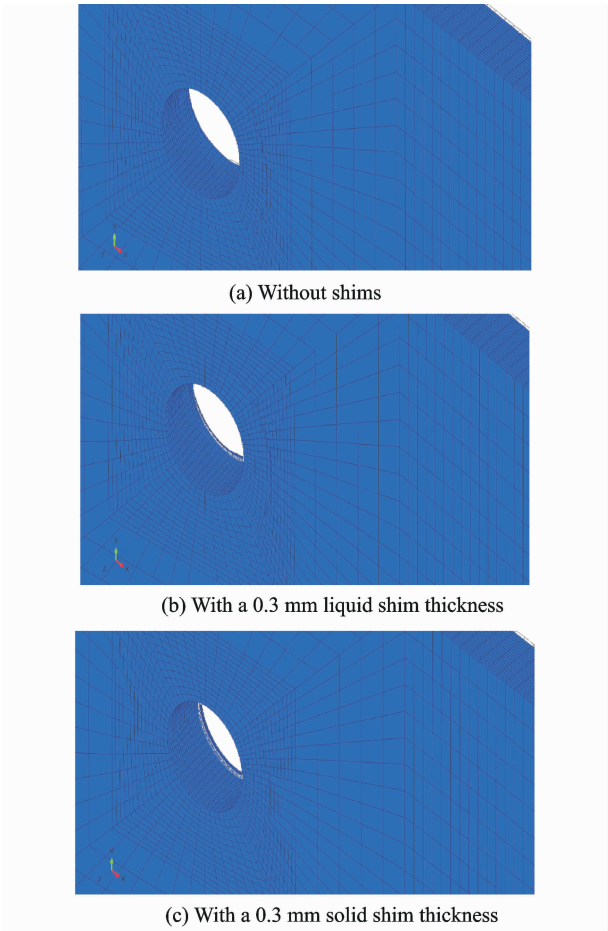

Fig. 28 FV4 damages for specimens without shim and with liquid and solid shim thicknesses

gate the influence of varying shim layers on the progressive damage/failure of a composite component in a bolted composite-aluminum aerospace structural assembly and the numerical results validated against the experimental results were generally in good agreement. From the analysis, the following was discovered:

(1) The shimming procedure as agreed upon by the aerospace industry for the resolution of assembly gaps in bolted joints for composite materials is same as that for a composite-aluminum structure: liquid shim series prolonged the service life of the composite component for the assembly gaps of 0.3, 0.5 and 0.7 mm; and a solid peelable fiberglass shim most had a better influence on the 0.9 mm assembly gap.

(2) The shim layers considerably influenced the structural strength of the composite component by delaying its failure, thereby increasing its service life.

(3) Increasing the shim layer's thickness led to a significant corresponding effect on the stiffness but with minimal effect on the ultimate load.

The aforementioned observations cannot be definitive because other factors, such as thermal expansion coefficients, failure, and fracture mechanisms, and degree of plasticity, might influence the trend observed in this paper for a composite-aluminum structure.

Acknowledgements

The authors wish to acknowledge the Innovation Foundation of National Research Center for Commercial Aircraft Manufacturing Engineering Technology in China (No. SAMC13-JS-13-021) and Jiangsu Key Laboratory of Precision and Micro-Manufacturing Technology for the provision of financial support.

References:

[1] MALLICK P K. Fiber-reinforced composites: Mate-

rials, manufacturing, and design[M]. 3rd Edition. New York:CRC Press, 2007:1-12.

[2] LAURIN F, CARRERE N, MAIRE J F. Strength analysis methods for high stress gradient parts in composite structures ensuring design office requirements[J]. Proc IMechE, Part G: J Aerospace Engineering, 2011,225(3):291-301.

[3] WALKER K. EASA widens AD for A380 cracks; Boeing confirms 787 shims[EB/OL]. [2012-02 08]/(2016-10-18). http://atwonline.com/aircraft-amp-engines/easa-widens-ad-a380-cracks-boeing-confirms-787-shims.

[4] FALZON B. The airbus A380 wing cracks: an engineer's perspective [EB/OL]. http://the conversation.com/the-airbus-a380-wing-cracks-an-engineers-perspective-5318. [2012-2-10](2016-10-18).

[5] KAPIDZIC Z. Strength analysis and modeling of hybrid composite-aluminum aircraft structures [D]. Linköping: Linköping University, 2013:3.

[6] CAMPBELL F C. Manufacturing technology for aerospace structural materials[M]. 1st Edition. Oxford: Elsevier Science and Technology, 2006: 498-499.

[7] TSAI S W, WU E M. A general theory of strength for anisotropic materials[J]. J Comp Mater, 1971, 5(1):58-80.

[8] REDDY J N, PANDEY A K. A first ply failure analysis of composite laminates [J]. Computers Struct, 1987,25(3):371-393.

[9] TURVEY G V. An initial flexural failure analysis of symmetrically laminated cross-ply rectangular plates [J]. Int J Solids Struct,1980,16(5):451-463.

[10] HASHIN Z. Analysis of cracked laminates: A variationalapproach[J]. Mech Mater, 1985, 4(2): 121-136.

[11] CHANG F K, CHANG K Y. A progressive damage model for laminated composites containing stress concentrations[J]. J Comp Mater, 1987,21(9):834-855.

[12] CHANG F K, LESSARD L B. Damage tolerance of laminated composites containing an open hole and subjected to compressive loadings: Part I—Analysis [J]. J Comp Mater, 1991,25(1):2-43.

[13] REDDY Y N S, REDDY J N. Linear and non-linear failure analysis of composite laminates with transverse shear[J]. Compos Sci Tech, 1992,44(3):227-255.

[14] KAPIDZIC Z, NILSSON L, ANSELL H. Finite element modeling of mechanically fastened composite-aluminum joints in aircraft structures[J]. Compos Struct, 2014,109:198-210.

[15] SMITH J. Concept development of an automated shim cell for F-35 forward fuselage outer mold line control [D]. Menomonie: University of Wisconsin-Stout, 2011.

[16] LEE R. Evaluation of shimming options with applications to JSF [EB/OL]. [1999-12]/(2016-11-21). http://materialchemistry.com/DreamHC/Download/JSF%20Shimming%20Analysis.pdf.

[17] CARACCIOLO P, KUHLMANN G. Reliability analysis in bolted composite joints with shimming material[C]//25th international congress of the aeronautical sciences. Hamburg, Germany, 2006: 524.

[18] HÜHNE C, ZERBST A K, KUHLMANN G, et al. Progressive damage analysis of composite bolted joints with liquid shim layers using constant and continuous degradation models [J]. ComposStruct, 2010,92(2):189-200.

[19] DHÔTE J X, COMER A J, STANLEY W F, et al. Study of the effect of liquid shim on single-lap joint using 3D digital image correlation[J]. ComposStruct, 2013, 96:216-225.

[20] COMER A J, DHÔTE J X, STANLEY W F, et al. Thermo-mechanical fatigue analysis of liquid shim in mechanically fastened hybrid joints for aerospace applications[J]. Compos Struct, 2012, 94(7): 2181-2187.

[21] DHÔTE J X, COMER A J, STANLEY W F, et al. Investigation into compressive properties of liquid shim for aerospace bolted joints[J]. Compos Struct, 2014,109:224-230.

[22] LIU L. The influence of the substrate's stiffness on the liquid shim effect in composite to titanium hybrid bolted joints[J]. Proc IMechE, Part G: J Aerospace Engineering, 2014, 228(3):470-479.

[23] ZHAI Y, LI D, LI X, et al. An experimental study on the effect of joining interface condition on bearing response of single-lap, countersunk composite-aluminum bolted joints[J]. Compos Struct, 2015, 134: 190-198.

[24] ASTM Standard D5961/D 5961M-13. Standard test method for bearing response of polymer matrix composite laminates [S]. West Conshohocken, PA, USA: ASTM International, 2013.

[25] ABAQUS. Inc. ABAQUS version 6.13 Documentation[M]. Velizy-Villacoublay: Dassault Systemes/SIMULIA, 2013.

[26] de LUCA, CAPUTO F, LAMANNA G, et al.

Study of analytical models for predicting impact damage to composite structures[C]// Italian Association for Stress Analysis 42nd National Congress. Salerno, Italy: University of Salerno, 2013: 11-14. (in Italian)

[27] ZHAO T W, JIANG Y. Fatigue of 7075-T651 aluminum alloy[J]. Int J Fatigue, 2008, 30(5): 834-849.

[28] SUN C T. Adhesively bonded joints, Part 1: bondline thickness effects and hybrid design of adhesively bonded joints[R]. DOT/FAA/AR-11/1, P1, USA: FAA report, February 2014.

[29] HARTMAN D R, GREENWOOD M E, MILLER D M. High Strength Glass Fibers: 1-Pl-19025-A[R]. Owens Corning Inc., Technical Paper Ref. July 1996. Reprinted by AGY LLC as Pub. No. LIT-2006-111, February 2006.

[30] STOCCHI C, ROBINSON P, PINHO S T. A detailed finite element investigation of composite bolted joints with countersunk fasteners [J]. Compos Struct: Part A, 2013, 52: 143-150.

[31] CHAKHERLOU T N, OSKOUEI R H, VOGWELL J. Experimental and numerical investigation of the effect of clamping force on the fatigue behaviour of bolted plates[J]. Eng Fail Anal, 2008, 15(5): 563-574.

[32] EKH J, SCHON J, MELIN L G. Secondary bending in multi fastener, composite-to-aluminium single shear lap joints[J]. Compos Struct: Part B, 2005, 36(3): 195-208.

[33] TSERPES K I, PAPANIKO P, KERMANIDIS T H. A three-dimensional progressive damage model for bolted joints in composite laminates subjected to tensile loading[J]. Fat Fract Engng Mater Struct, 2001, 24: 663-675.

[34] LIU L, ZHANG J, CHEN K, et al. Combined and interactive effects of interference fit and preloads on composite joints[J]. Chin J Aero, 2014, 27(3): 716-729.

Mr. **Attahu Cephas Yaw** graduated with a B. Sc. degree in aerospace engineering in June 2013 from Kwame Nkrumah University of Science and Technology (KNUST), Ghana. He served as a teaching assistant with the department of Mechanical Engineering, KNUST, Ghana from August 2013 to August 2014 before joining the department of Aerospace Manufacturing Engineering, Nanjing University of Aeronautics and Astronautics (NUAA), in September 2014 as a master student for a 2.5 years' programme which ends in April 2017. His primary research interest is aircraft assembly technology.

Prof. **An Luling** received his B. Sc. degree in mechanical design from Nanjing University of Aeronautics and Astronautics (NUAA) in 1982. He had his M. Sc. degree in mechanics from Shangdong University of Science and Technology in 1985 and his Ph. D. degree in aerospace manufacturing engineering in 2001 from NUAA. He is a full professor with the department of aerospace manufacturing engineering and has been with the department since 2001. His research is focused on digital design and manufacturing technology, virtual manufacturing technology and aircraft assembly technology.

Ms. **Li Zhaoqing** is an assistant engineer in Structural Strength Institute of Xi'an Aircraft Design Institute, AVIC Xi'an Aircraft Industry(Group) Company LTD, who graduated from the Northwest Polytechnical University with a major in flight vehicle design and engineering.

Mr. **Gao Guoqiang** is a Ph. D. student of aerospace manufacturing engineering, NUAA. His research focuses on the assembly of composite aircraft structures.

(Production Editor: Zhang Tong)